Journal of Structural Geology, Vol. 13, No. 5, pp. 595 to 608, 1991
Printed in Great Britain

0191-8141/91 $03.00+0.00

The initiation and growth of en échelon veins

JON E. OLSON* and DAVID D. POLLARD

Department of Applied Earth Sciences, Stanford University, Stanford, CA 94305, U.S.A.

(*Received* 27 *March* 1990; *accepted in revised form* 19 *October* 1990)

Abstract—Numerical models are used to understand the evolution of mode I (opening) fractures from spatially random distributions in a brittle elastic material. En échelon arrays commonly develop because mechanical fracture interaction promotes growth for this geometry. This provides a new mechanism for en échelon vein formation in rock which is distinctly different than previously proposed mechanisms. It is suggested that some macroscopic en échelon vein arrays may have served as zones of weakness that localized later shear zone development in a manner analogous to that observed by experimentalists examining micro-cracking and subsequent shear rupture of rocks loaded under compression. Sigmoidally shaped veins and vein fillings are explicitly modeled showing that they can form in response to the mechanical interaction of neighboring fractures which redirects the propagation path. Numerical comparison of sigmoidal veins formed by brittle fracture and by ductile shear zones demonstrates some of the pitfalls of failing to correctly identify the mechanism of formation.

INTRODUCTION

TRADITIONALLY, en échelon veins have been attributed to an applied shear deformation: the experiments of Riedel (1929) and Cloos (1955) showed how these structures might form. The experiments involved building a clay cake over two parallel boards. As one board was slid past the other, simulating a narrow fault, a broad zone of shear deformation and fracturing developed in the overlying clay cake. If water was sprinkled liberally on the surface of the clay cake, opening fractures (referred to by different authors as 'tensile', 'dilatant', or 'extensional' fractures or 'tension gashes') formed along the fault line, oriented approximately 45° from the fault trend (Fig. 1a). Due to passive rotation of the central portion of fractures in the deformation zone and continued growth at the fracture tips, sigmoidal shapes sometimes formed (Fig. 1b).

Shainin (1950) described vein systems in the Athens limestone of Virginia which he inferred were formed by the action of a shear couple on an incipient shear failure plane. The maximum compressive stress direction was interpreted to be the acute bisectrix between conjugate vein arrays. Shainin concluded that the veins were 'tensile' fractures having initiated on planes approximately 45° from the shear zone boundary. Shainin observed that shear offset across the zones was common and suggested the sigmoidal shapes of some veins indicated rotational deformation within the zone due to shearing. Wilson (1952) described similar geometric features in quartz veins of the Moine Series of Scotland, and concluded that interlayer slip during folding applied shear couples to the rock layers, resulting in en échelon 'tension gashes' forming at acute angles to layer boundaries.

Roering (1968) observed that many en échelon vein arrays exhibit no measurable shear offset and suggested that veins may pre-date shear zone formation. He rejected an earlier idea that these en échelon veins were responding to a modified local (secondary) stress state caused by shear zone formation (Shainin 1950, Wilson 1952, Cloos 1955). Instead, Roering claimed that the veins he observed could be directly related to the remote (primary) stress state as a type of 'shear' fracture. In contrast, Lajtai (1969) asserted that there must be a pre-existing zone of weakness such as a shear zone in order

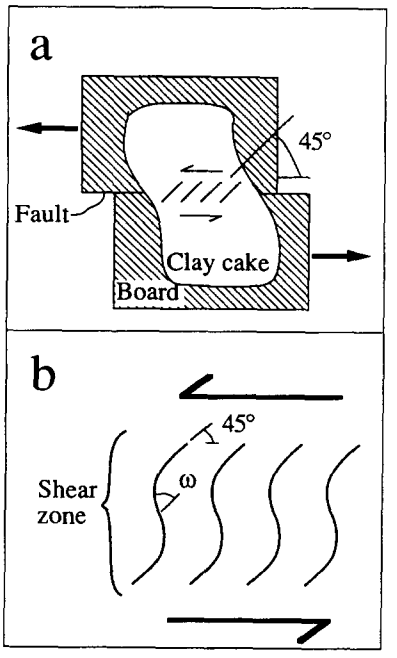

Fig. 1. Illustration of clay cake experiments of Riedel (1929) and Cloos (1955). (a) Clay cake being deformed over two displacing boards, simulating a buried fault. The shear displacement of the 'fault' translates into a broad zone of deformation in the clay, causing tension gashes oriented at about 45° to the applied shear motion (when the clay is wet). (b) Finite rotation in the deformation zone causes the central portion of the tension gashes to rotate through an angle ω while continued propagation at the fracture tips maintains about a 45° angle with the zone boundaries, resulting in sigmoidally shaped fractures.

*Present address: Mobil Research and Development Corporation, 13777 Midway Road, Dallas, TX 75244, U.S.A.

to localize veins in en échelon arrays. He concluded that veins form as 'tension' fractures aligned with the local stress field within a shear zone so they cannot be used directly to infer remote stress directions. However, Lajtai interpreted the sigmoidal shape of some veins to indicate growth outside the boundary of a shear zone and inferred that the tips of these veins would most likely be aligned with the remote stress directions.

Hancock (1972) accepted Lajtai's shear zone hypothesis and went on to classify en échelon veins into three failure categories based on their vein-array angle, δ (Fig. 2). He proposed that fractures analogous to those described by Riedel (1929) from his clay experiments, termed 'Riedel shears', form at 10–20° to a shear zone. 'Transitional shear-extension' fractures form at 20–40°, and 'extension' fractures form at 40–45°. Beach (1975) narrowed the categories of en échelon veins to two: (1) 'shear' fractures that form after the shear zone; and (2) 'tensile' fractures that localize in arrays independent of shear zones due to an unspecified mechanism. According to Beach, the shear fractures should be parallel to the trend of the adjacent conjugate array, although he admitted that later rotations may obscure this relationship. The 'tensile' fractures were hypothesized to have small vein-array angles, but again it was allowed that the angles may vary due to later shearing and rotation.

Ramsay (1980) used a kinematic analysis to explain the variation in vein-array angles. Instead of relying on a change in failure mechanism as proposed by Beach (1975), he interpreted the vein geometry variations as an outgrowth of volume changes superimposed on simple shear deformation. Ramsay suggested that shear zones with positive dilatation ($\Delta_v > 0$, Fig. 3a) should exhibit $\delta < 45°$ while those with negative dilation ($\Delta_v < 0$, Fig. 3b) should have $\delta > 45°$. Arrays formed during simple shear alone should have $\delta = 45°$. Rickard & Rixon (1983) applied Ramsay's theory to certain field observations and also postulated that some shear zones were made up of hybrid 'extensional/shear' fractures as predicted by failure envelopes on a Mohr diagram, an interpretation similar to that of Hancock (1972). Yet Rickard & Rixon rejected the hypotheses of Roering (1968) and Beach (1975) that the veins can be primary 'shear' fractures.

Lajtai (1969), Rickard & Rixon (1983), and many others have considered en échelon veins to form only as a result of shear zone deformation. However, Pollard *et al.* (1982) proposed a mechanism for en échelon arrays with modest vein-array angles that is independent of shear zones. Based on experiments by Sommer (1969), they called upon a temporal or spatial rotation of the principal stress field about an axis parallel to the propagation direction of a 'dilatant' parent fracture. The loading scheme used by Sommer achieves this rotation by a torque applied to a rod in axial tension (Fig. 4a). This corresponds to a mixture of mode I (opening) and mode III (shearing parallel to the fracture tip) loading (Lawn & Wilshaw 1975). Since 'dilatant' fractures tend to grow in a principal stress plane, this stress rotation requires some rotation of each successive increment of

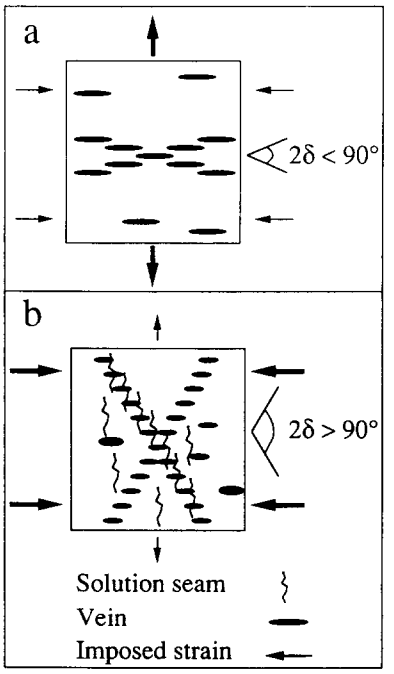

Fig. 3. Inferred dependency of vein-array angle on bulk shape changes and dilatation, Δ_v (after Ramsay & Huber 1987, fig. 26.42). (a) Stretching and shortening, $\Delta_v > 0$, shear zones with small vein-array angles, $2\delta < 90°$, no pressure solution. (b) Stretching and shortening, $\Delta_v < 0$, shear zones with large vein-array angles, $2\delta > 90°$, significant pressure solution.

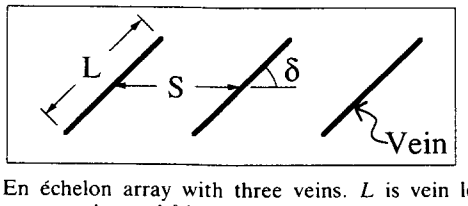

Fig. 2. En échelon array with three veins. L is vein length, S is separation and δ is termed the vein-array angle.

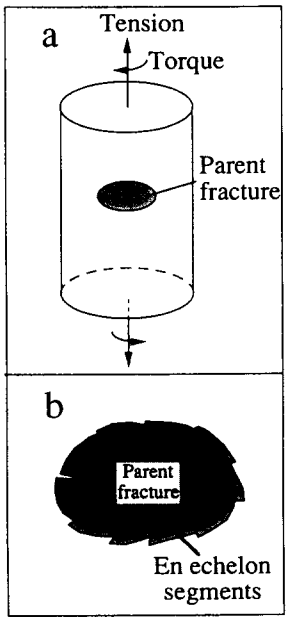

Fig. 4. Experiment of Sommer (1969). (a) Tension and torque applied to glass rod with embedded penny-shaped fracture. The loading on the crack is mixed mode I–III in the terminology of engineering fracture mechanics. (b) Resulting crack propagation, showing breakdown of parent crack into rotated en échelon segments.

fracture growth. Due to energy constraints (Pollard *et al.* 1982), the parent fracture (Fig. 4a) breaks down into en échelon segments (Fig. 4b) in a manner similar to twist hackle and fringe joints (Woodworth 1896, Hodgson 1961, Bankwitz 1965). Possible examples of this mechanism for vein formation are described in Knipe & White (1979), Granier (1985) and Shaoxun & Xiaoshuang (1988). Delaney & Pollard (1981) and Pollard *et al.* (1982) also have applied this concept to the interpretation of en échelon dikes.

Pollard *et al.* (1982) proposed that some features supposed to be diagnostic of vein arrays in shear zones, such as sigmoidal shapes, shear displacement of the vein-wall, and apparent shear offset across the array, can result simply from 'dilatant' fracture growth. A method to confirm this hypothesis has been developed by Craddock & van der Pluijm (1988) using detailed petrofabric analysis of vein-filling material. They examined the strain variation in an array of sigmoidal 'tension gashes' that change laterally into a single continuous vein. They concluded that the sigmoidal shapes were due to vein propagation in a locally varying stress field caused by mechanical fracture interaction. They found no evidence to support the more traditional interpretation of growth at the vein tips aligned with the remote stress directions and finite rotations of the vein centers within a 'shear zone'.

Rothery (1988) recently proposed a new classification system for en échelon veins. His data, collected from the Lower Carboniferous limestones in the SE midlands of Ireland, showed en échelon veins with a range of vein-array angles from approximately 5° to 55°. He attributed arrays with $\delta < 27°$ to the mode I–III breakdown of dilatant parent fractures into en échelon segments after Pollard *et al.* (1982). All other arrays were considered to be a result of shear zone formation, but the diagnostic features associated with either mechanism were not abundant. Rothery stated "the majority of arrays sampled provide no clear evidence of having developed from a parent extensional crack or from a zone of localized shear strain" (1988, p. 67). Thus, his interpretation, as that of many others, relied almost exclusively on the magnitude of vein-array angles and their inferred genetic link with the two different mechanisms of origin.

The foregoing summary of previous work exemplifies the long-running controversy concerning the interpretation of en échelon veins. It should be clear to anyone familiar with this literature that more than one mechanism can produce en échelon veins. Since field observations and theory suggest different mechanisms result in similarly shaped veins, interpretations based solely on limited aspects of vein geometry (i.e. the magnitude of vein-array angles or the presence of conjugate arrays) can be problematic. In addition, fracture analyses based upon homogeneous stress field representations (such as those done with Mohr circles and Mohr–Coulomb failure envelopes) are almost certainly inadequate because of the strong dependence of fracture propagation direction on the highly heterogeneous local stress fields typical of fracture tips.

A new perspective

In this paper, we advocate an approach for interpreting en échelon vein arrays based on the solutions of the appropriate boundary and initial value problems of continuum mechanics. Inherent in these solutions are the explicit relationships among the displacement, strain, and stress fields lacking in much of the previous work. We also propose a new mechanism for the formation of some en échelon vein arrays based upon numerical experiments in which opening fractures grow as governed by the principles of fracture mechanics. This single mechanism can account for the full range of vein-array angles reported in the literature (approximately 0–55°) and brings into question interpretive methods which have used these angles as the primary evidence for distinguishing other mechanisms of origin.

Whereas previous analytical methods, most utilizing the Mohr diagram, dealt only with the homogeneous stress state in a body prior to fracturing, the proposed mechanism is supported with modeling that explicitly includes the fractures and their resultant heterogeneous fields. With this modeling we reproduce commonly observed features, such as sigmoidal vein shape, shear displacements across veins, and en échelon arrays, as by-products of remote loading that is constant in orientation and purely extensional. We illustrate why an en échelon zone with a particular vein-array angle, δ, does not necessarily imply the existence of a shear zone or a mixed mode I–III loading of a parent opening fracture. In addition, even where obvious evidence of shearing deformation exists, we provide support for the view of Roering (1968) that en échelon veins may sometimes be the precursor to, and not the result of, localized shear deformation.

Our work on the proposed mechanism for en échelon veins was foreshadowed by laboratory experiments on cylindrical rock specimens loaded in triaxial compression in which tensile micro-cracking precedes shear failure (Brace & Bombolakis 1963, Peng & Johnson 1972, Dunn *et al.* 1973, Hallbauer *et al.* 1973, Sobolev *et al.* 1978, Wong 1982, Kranz 1983). Direct observations and acoustic emission studies demonstrate the micro-cracking may be spatially random at first, but crack orientation is typically parallel to the maximum compressive principal stress (Brace *et al.* 1966, Tapponier & Brace 1976, Sangha *et al.* 1974, Olsson & Peng 1976, Kranz 1979). The cracks' orientation is perpendicular to the least compressive stress, consistent with their interpreted opening mode origin. Continued axial compression of the rock sample is accompanied by the localization of micro-cracks and other deformation features in narrow, sometimes conjugate diagonal bands with subsequent shear rupture across these zones of weakness. The formation of the conjugate arrays of axial cracks has been attributed to the heterogeneous stress distribution caused by the end effects on the specimen (Peng & Johnson 1972), and to the mechanical interaction of nearby micro-cracks which favors en échelon growth (Dey & Wang 1981). In the latter case, the most prob-

able orientation of the array depends upon the distance between existing micro-cracks relative to their lengths.

We postulate that the mechanical interaction of fractures as outlined by Dey & Wang (1981) can be used to explain the development of en échelon arrays at scales ranging from laboratory specimens to crustal blocks, but we will concentrate on the outcrop scale features of veins in this paper. Work at this scale is, in many respects, a more straightforward application of the continuum methods than the aforementioned micro-crack problem. There, the material heterogeneities due to the granular nature of most rock specimens are more pronounced than those associated with many rock masses at the outcrop scale. Similarly, the material anisotropies common to many rock forming minerals often are not found at the outcrop scale. Thus, we can justify the simplifying postulates of homogeneity and isotropy with more confidence, while recognizing that these postulates will have to be relaxed in some cases.

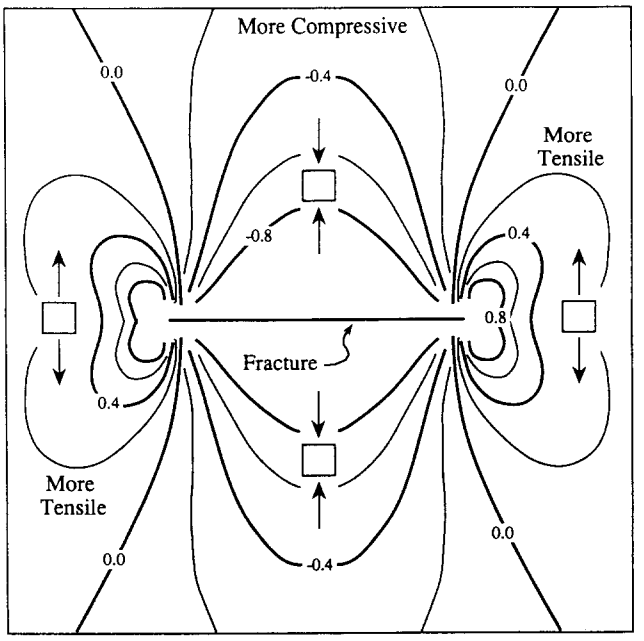

Fig. 5. Distribution of crack perpendicular stress, σ_{yy}, induced by a fluid-pressurized crack. Contours are labeled with stress magnitude normalized by the fluid pressure (tension is positive). Crack-induced stress is tensile in front of the crack tips and compressive to either side of the crack.

FRACTURE-INDUCED STRESS FIELDS

Consider a uniformly loaded body composed of homogeneous and isotropic rock and containing a set of fractures. Each fracture will locally perturb the applied stress field in a complex manner (Pollard & Segall 1987), but, if a particular fracture is isolated from its neighbors by distances that are large compared to the fracture lengths, it will be surrounded by and acted upon by a spatially uniform field. This so-called *remote stress field*, in conjunction with the internal fluid pressure, controls the onset and path of propagation of the isolated fracture. If the fracture is oriented perpendicular to the minimum compressive stress of this remote field, it will open in pure mode I when its internal fluid pressure exceeds this stress component. The fracture will propagate along a straight path when the stress concentration at its tip exceeds the rock strength.

In contrast, if the fracture in question is not isolated from its neighbors, the stress perturbations induced by nearby fractures will influence the onset and path of propagation. We refer to these effects as *mechanical fracture interaction*. Because both normal and shear stress components can be induced on the fracture plane by neighboring fractures, the resulting loading may not be pure mode I and the propagation path may not be straight. To understand the nature of fracture interaction, it is helpful to examine the stress field induced by a single fracture after subtracting out the effects of the uniform remote field using the principle of superposition for linear elasticity (Timoshenko & Goodier 1970, p. 243). Figure 5 shows the fracture-induced contribution to the normal stress component, σ_{yy}, about an isolated, pressurized fracture (Pollard & Segall 1987). The stress contours are normalized by the magnitude of the difference between the fluid pressure in the fracture and the remote minimum compressive stress. This difference is referred to as the *driving stress* (Pollard & Segall 1987). The variations in magnitude of σ_{yy} will influence the growth of nearby fractures that are parallel to the perturbing fracture.

For a given distance from the fracture tip (away from the near-tip region), the maximum value of σ_{yy} occurs along lines approximately $\pm 45°$ ahead of the crack. If we postulate the existence of a population of randomly located micro-cracks parallel to the maximum compressive stress and to the 'master' fracture of Fig. 5, we would expect preferential growth of those microcracks located along diagonal lines ahead of the tip of the existing master fracture, forming an en échelon array. Many examples of en échelon arrays apparently grow in the absence of the stress perturbation of a larger master fracture and form approximately equal-sized veins. Using numerical experiments, we will show how mechanical interaction can have a controlling influence on fracture propagation patterns from a random distribution of comparably sized flaws and favors the growth of en échelon arrays.

RESULTS FROM NUMERICAL EXPERIMENTS

We performed numerical experiments modeling the growth of opening fractures for various initial geometries in order to test the hypothesis that interaction will favor en échelon array formation. The experiments were done using a two-dimensional, plane strain boundary element computer code (modified from Crouch & Starfield 1983) incorporating a linear elastic fracture propagation criterion (Erdogan & Sih 1963, Ingraffea 1981). All modeled fractures were divided into displacement discontinuity elements (dislocations) of constant length (here designated one length unit), with an additional element of the same length added at the fracture tip for

each propagation increment. Each element can sustain a constant normal and/or tangential displacement discontinuity which corresponds to the opening or shearing of that portion of the fracture.

Propagation force for en échelon veins

We examine a single en échelon array of straight fractures to illustrate the controlling parameters of fracture growth. The loading at the fracture tip is summarized by the fracture propagation force, G, and is calculated as a function of the mode I (opening) and mode II (shearing) stress intensity factors, K_I and K_{II}. The stress intensity factors measure the stress concentration at the fracture tip, and depend upon the fracture geometry and applied loading conditions. For an isolated, straight fracture (Fig. 6), the expressions for the fracture propagation force and stress intensity factors take on a simple form (Lawn & Wilshaw 1975),

$$G = \frac{1}{E}(K_I^2 + K_{II}^2) \quad (1)$$

$$K_I = \Delta\sigma_I \sqrt{\pi a} \quad (2)$$

$$K_{II} = \Delta\sigma_{II} \sqrt{\pi a}, \quad (3)$$

where a is fracture half-length, E is Young's modulus, and the driving stresses, $\Delta\sigma_I$ and $\Delta\sigma_{II}$, are defined as

$$\Delta\sigma_I = \sigma_{yy}^r - \sigma_{yy}^c \quad (4)$$

$$\Delta\sigma_{II} = \sigma_{xy}^r - \sigma_{xy}^c. \quad (5)$$

The superscripts r and c refer to remote and crack face stresses, respectively (tension is positive and fluid pressure is negative). Pure mode I opening of the fracture results when $\sigma_{yy}^r > \sigma_{yy}^c$ (e.g. internal fluid pressure exceeds remote compressive stress or the remote normal stress is tensile) and $\sigma_{xy}^r = \sigma_{xy}^c = 0$. Pure mode II shearing occurs when $\sigma_{xy}^r \neq \sigma_{xy}^c$ and $\sigma_{yy}^r = \sigma_{yy}^c$ (e.g. net shear exceeds frictional strength across a closed fracture). Mixed mode I–II deformation, involving a combination of opening and relative shearing displacements of the fracture walls, is the expected general case because

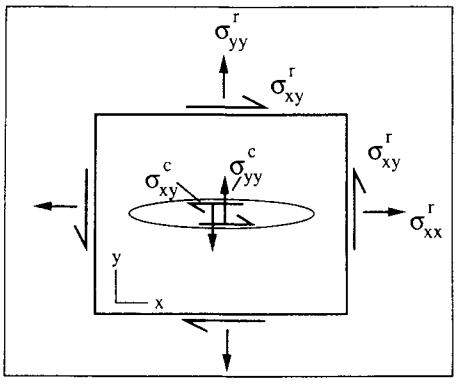

Fig. 6. Definition of stress components for an isolated fracture in an infinite body. σ_{xx}^r and σ_{yy}^r are the remote normal stresses, σ_{xy}^r is the remote shear stress, σ_{yy}^c is the uniform normal traction acting on the crack face, and σ_{xy}^c is the uniform shear traction on the crack face. Driving stress for opening mode crack propagation is defined as $\Delta\sigma_I = (\sigma_{yy}^r - \sigma_{yy}^c)$. All stresses shown have a positive sign, thus remote tension is positive and pressure in the crack is negative.

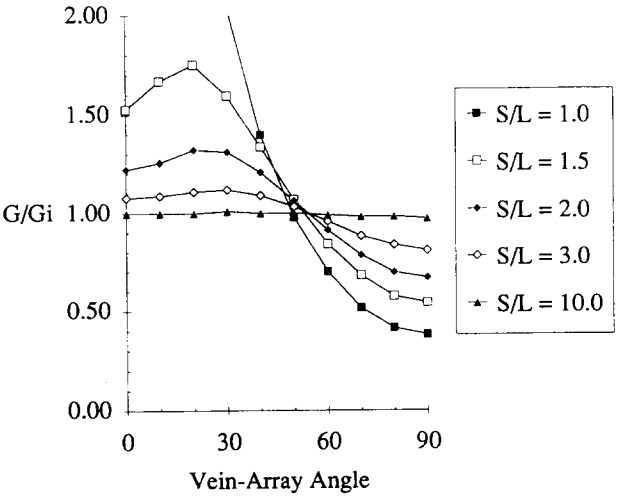

Fig. 7. Crack propagation ratio, G/G_i, plotted against vein-array angle, δ, for various normalized separations, S/L (see Fig. 2). $G/G_i > 1$ indicates enhanced fracture propagation due to interaction, $G/G_i < 1$ indicates hindered crack propagation. A collinear array has a vein-array angle of $\delta = 0°$, and a stacked array has $\delta = 90°$.

mechanical interaction will induce normal and shear stresses on neighboring fractures. Mixed mode loading may result in curved propagation paths and complicated fracture wall displacement histories, as the fracture tip will tend to grow perpendicular to the orientation of the local least principal stress.

The elastic fields were calculated for en échelon arrays containing five straight, fluid pressurized fractures with various center-to-center separations to determine the optimal fracture-array angle, δ (see Fig. 2). The remote boundary conditions were constant isotropic stress. The ratio of fracture separation to length, S/L, ranged from 1 to 10. The fracture propagation force, G, for the middle member of a five fracture array is normalized by G_i, that for an isolated fracture of the same length. This normalized value will be called the 'propagation ratio' and allows us to judge whether propagation is enhanced, $G/G_i > 1.0$, or hindered $G/G_i < 1.0$, due to fracture interaction for the specified geometry.

The optimal vein-array angle for a particular separation, S/L, is indicated by the maximum value of G/G_i (Fig. 7). For $S/L = 1$, the optimal configuration is at $\delta = 0°$ due to the tip-to-tip linking of fractures. The optimal angle for $S/L = 1.5$ is an array with $\delta \approx 20°$ and a propagation ratio of about 1.8. The propagation ratio drops quickly from this peak value to a minimum of about 0.6 for $\delta = 90°$, a configuration we will term a 'stacked' array. The lowest propagation ratio was about 0.4 for $S/L = 1.0$ and $\delta = 90°$. As separations increase, the optimal angle increases to a maximum of approximately 30° for $S/L = 3$ and $S/L = 10$. In general, however, for all arrays with δ less than about 50° the propagation ratio is greater than 1.0 and thus growth would be enhanced due to mechanical interaction. The opposite is true when δ is greater than about 50°; for these geometries, fracture interaction would hinder growth.

The effects of separation on fracture interaction are evident by comparing the results for the various S/L

ratios in Fig. 7. Interaction effects are most significant for fractures with the smallest separations because this geometry brings the two near-tip stress concentrations closest together. As separations increase, the maximum and minimum values for the propagation ratios are closer to 1 and the curves are flatter. The results show enhancements of the propagation ratio for the optimal array relative to a stacked array of 300, 180 and 40% for S/L of 1.5, 2 and 3, respectively. The results for $S/L = 10$ show that fracture arrays of all orientations behave almost as if the fractures were isolated.

Another parameter affecting propagation force is fracture length. Since G increases linearly with length, given similar loading, longer fractures are always favored for growth over shorter ones. Because fractures in certain en échelon geometries have a greater G due to interaction effects (Fig. 7), these fractures will grow first and will be favored for further propagation due to a greater length. Longer cracks also cast stronger and more extensive compressive stress shadows (Fig. 5), hindering shorter cracks to their sides from propagating. We propose that this complex mechanical interplay favors the initiation of en échelon arrays and explains, in part, why they are so common. The great resistance to further growth of overlapped échelon fractures (Pollard *et al.* 1982, fig. 12a) explains why so many arrays are 'frozen' into the rock record.

Vein-array angles

To evaluate the importance of en échelon array initiation due to mechanical interaction, we performed numerical model experiments using randomly located, equal-length, parallel fractures. The initial fractures were 0.1 m in length and were divided into 0.05 m boundary elements. Subsequent growth on the fractures was in 0.05 m increments at either tip. The surface area of the representative volume of fractured rock was 100 m^2. A set of 100 experiments was performed, half with 50 starting fractures and half with 100 starting fractures representing initial fracture densities of 0.00125 and 0.00250, respectively (Segall 1984). Differences in the amount of fracture propagation between fractures of a given experiment can be attributed solely to the effects of mechanical interaction. The amount of total fracture growth in an experiment was limited by available computer time and memory, so the models with higher initial fracture density have, on average, shorter final fracture lengths. A typical experiment consumed about 100 cpu minutes on a Gould 9080, a computer rated at 10 MIPS.

The stress boundary conditions used for the numerical models consisted of $\sigma^r_{xx} = -21$ MPa, $\sigma^r_{yy} = -20$ MPa, $\sigma^r_{xy} = 0$ MPa, $\sigma^c_{yy} = -24.7$ MPa, and $\sigma^c_{xy} = 0$ MPa. This results in a differential remote compression of 1 MPa parallel to the starting fractures, and a driving stress of 4.7 MPa. These are stresses that might be representative of *in situ* conditions in the upper 2 km of the Earth's crust. Numerically, propagation involved adding a single boundary element per iteration to either end of a fracture as specified by the maximum circumferential stress theory (Erdogan & Sih 1963). This failure criterion states that propagation should occur along a path across which circumferential tension, $\sigma_{\theta\theta}$, near the crack tip is maximized and resolved shear stress, $\sigma_{r\theta}$, is zero (Fig. 8). At each iteration the incremental propagation direction, θ, is defined by the equation

$$K_I \sin\theta + K_{II}(3\cos\theta - 1) = 0. \quad (6)$$

A fracture propagates when the stress intensities and propagation angle satisfy the inequality

$$\cos\frac{\theta}{2}\left(K_I \cos^2\frac{\theta}{2} - \frac{3}{2}K_{II}\sin\theta\right) \geq K_{Ic}, \quad (7)$$

where K_{Ic} is a material property called the fracture toughness (Lawn & Wilshaw 1975). For these experiments, we used a fracture toughness of 1.9 MPa-m$^{1/2}$, a representative laboratory determined value for sedimentary rock (Atkinson & Meredith 1987).

Two fracture patterns (Figs. 9a & b) from different starting populations clearly illustrate the effects of fracture interaction. Not all of the fractures grow in any particular experiment. For example, interaction prevented growth for some closely spaced stacked arrays (Fig. 9a, areas a & b; Fig. 9b, area a). Also, a lack of interaction because of the great spacing prevented some en échelon pairs from propagating (Fig. 9b, areas b & c). On the other hand, en échelon arrays with a wide variety of angles δ did grow (Fig. 9a, areas c–e; Fig. 9b, areas d & e). Since the driving stress for these experiments was large relative to the fracture-parallel differential compression, fracture path curving occurred in places where nearby fractures overlapped (Olson & Pollard 1989). This gave a sigmoidal shape to some of the fractures (Fig. 9a, areas c & d; Fig. 9a, areas d & e).

We have summarized the results of all 100 numerical experiments and quantified the vein-array angular relationships that promote and hinder fracture growth by measuring the normalized separations, S_i/L_o, and vein array angles, δ_i, for all neighboring fracture pairs (Fig. 10). Here we define the neighborhood of a particular fracture as the circular area centered on the fracture with a radius of 10 times the starting fracture length, L_o. Figure 11 shows the total number of possible fracture pairs within 5° increments over the range of $0° \leq \delta \leq 90°$

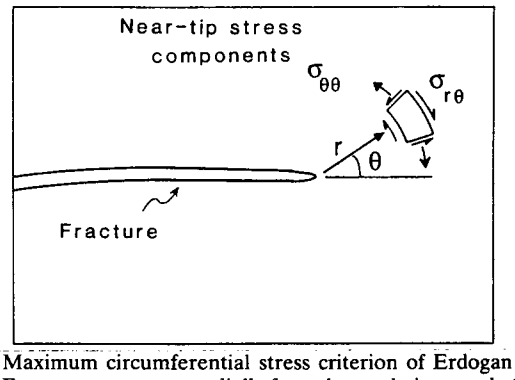

Fig. 8. Maximum circumferential stress criterion of Erdogan & Sih (1963). Fractures propagate radially from the crack tip at angle θ along a path of maximum circumferential stress, $\sigma_{\theta\theta}$, and zero shear stress, $\sigma_{r\theta}$.

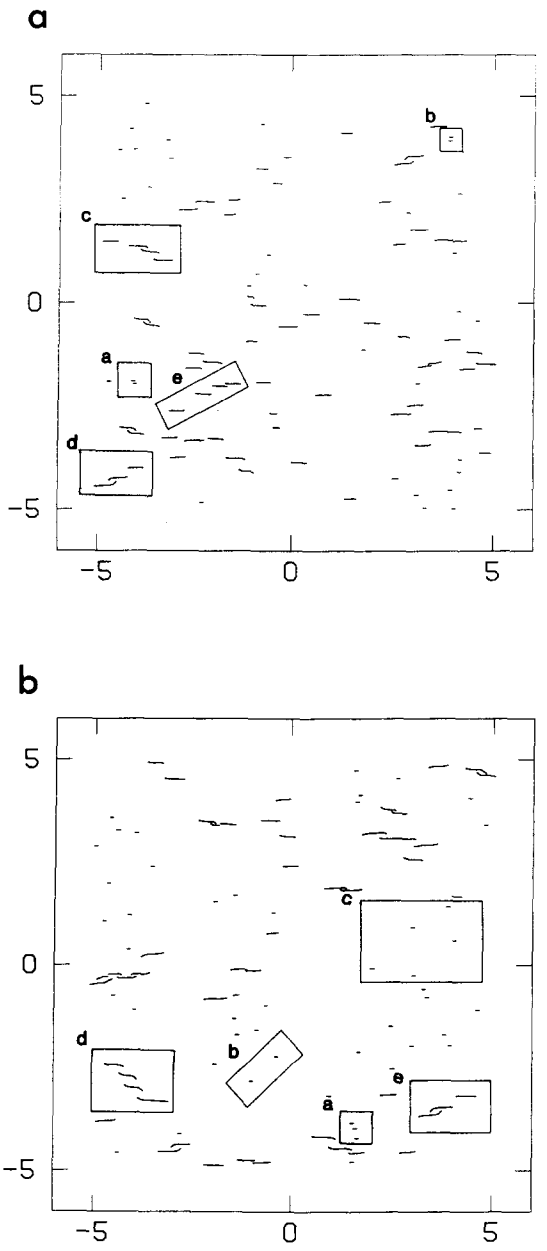

Fig. 9. Fracture patterns generated from 100 randomly located, parallel starting, fractures of equal length. The two patterns were generated from different initial fracture distributions. All cracks experienced the same remote stress and internal fluid pressure, but crack interaction caused some to grow and prevented others. Boxed regions highlight en échelon and stacked arrays referred to in the text. (a) Areas a and b show how stacked arrays are prevented from growth due to hindering interaction, and areas c–e show how en échelon arrays are favored for growth. (b) Area a exhibits a non-growing stacked array. Areas b and c show en échelon arrays with fractures that are too widely separated to cause sufficient constructive interaction to cause growth, while the more closely spaced en échelon fractures of d and e do grow.

for the three specified ranges of S/L_o. Fracture pairs with $90° < \delta < 360°$ are included in the 0–90° range using the two-fold symmetry of the stress field around an isolated fracture (Fig. 5). Spatial randomness for the starting fractures resulted in a wide range of crack separations, and the possible vein-array angles are distributed evenly throughout the range of orientations.

Using the tally of possible pairs and the results of the numerical experiments, we calculated the percentage that actually grew within each population defined by the

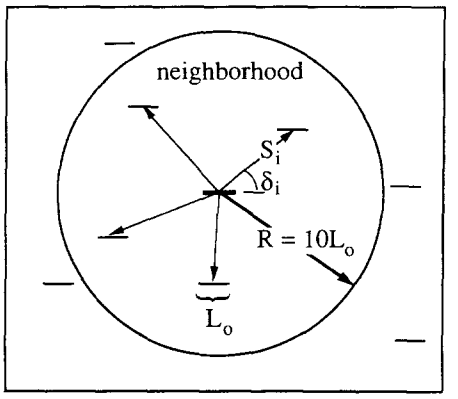

Fig. 10. Fractures from numerical experiments (e.g. Fig. 8) are grouped into pairs that have a separation, S_i, and a fracture-array angle, δ_i. Fractures are paired only with their nearest neighbors, those within a radial distance of 10 starter fracture lengths, L_o.

δ and S/L_o ranges in order to determine whether opening mode fracture growth favored en échelon array development. In general, Fig. 12 shows that arrays with $\delta < 50°$ are favored for growth relative to arrays with $\delta > 50°$. For arrays with small separations ($S/L_o < 5$) and modest vein-array angles ($\delta < 45°$), the percentage of fractures that grew is very high (75–100%). The percentage of growing fractures with $\delta > 70°$ drops below 30% for all separations. For $\delta < 55°$ it is evident that increas-

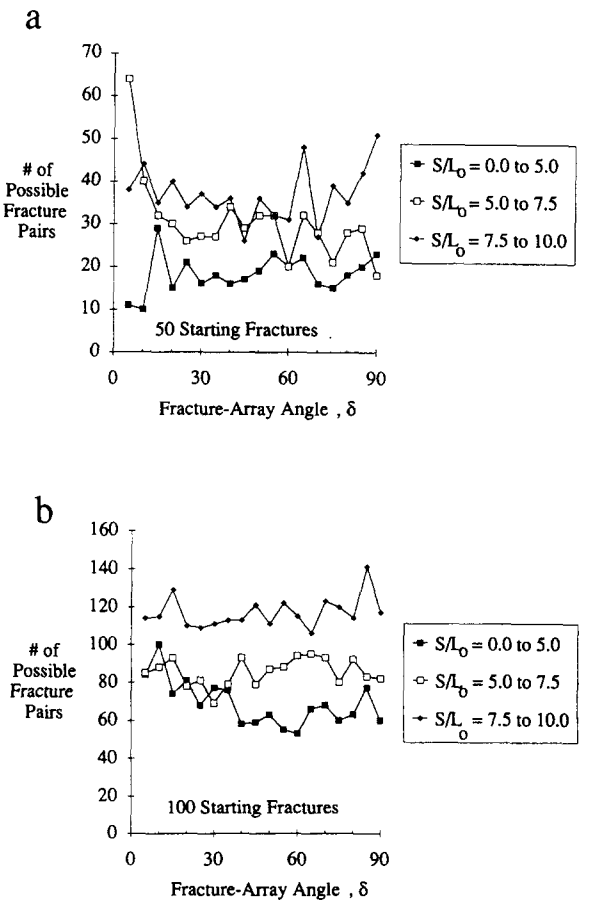

Fig. 11. Total number of fracture pairs for given ranges of separation, S/L_o, and 5° increments of fracture-array angle. (a) Fracture pairs for the experiments using 50 starter fractures. (b) Fracture pairs for the experiments using 100 starter fractures.

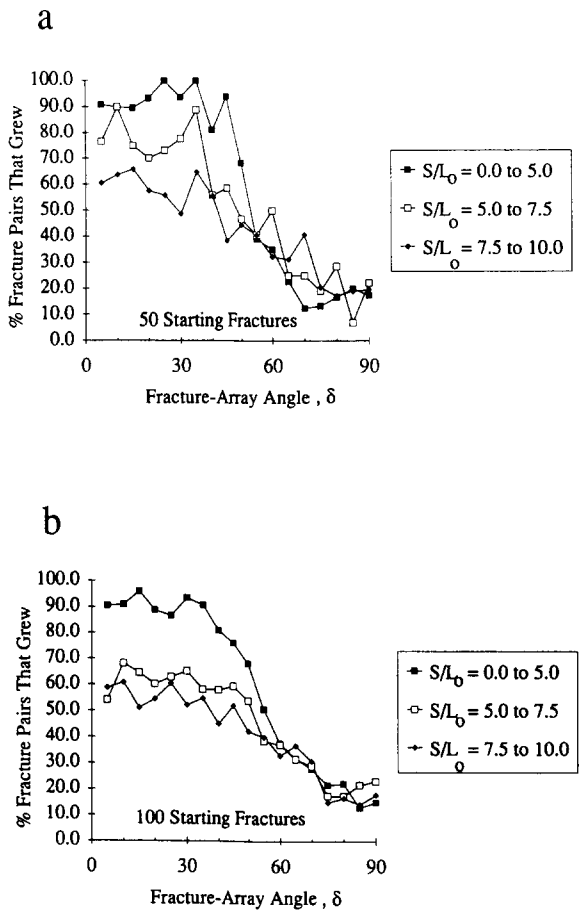

Fig. 12. Percentage of fracture pairs that grew in numerical experiments plotted vs fracture-array angle, δ, for three different normalized separations S/L_0. (a) Results of the numerical experiments using 50 starter fractures. (b) Results of the numerical experiments using 100 starter fractures.

ing separation diminishes positive interaction effects that promote growth. The similarity between the 50 and 100 fracture experiments as compared in Figs. 12(a) & (b) indicates that fracture density did not significantly affect the results. Also, although not depicted here, other numerical experiments indicate that the type of loading conditions applied to stimulate fracture growth, whether constant stress or constant displacement, do not alter the fracture-array angle results appreciably.

The analysis of five en échelon fractures (Fig. 7) indicates a rather sharp cut-off at about $\delta = 50°$ separating favored and unfavored configurations, whereas the numerical experiments with random fractures suggest a range of cut-off angles from about 45° to 55°. Like those cases of Fig. 7 with greater separation, the random fracture growth curves of Fig. 12 are fairly flat for $0° < \delta < 45°$. However, the random models show a stronger growth hindrance than is implied by the results for the five fracture array. This may be explained by the fact that a finite fracture strength was employed in the random models. Since the applied loading was raised only to the level that caused the most favorably situated fractures to grow, even very small negative interaction inhibited other fractures, thus skewing the results toward lower percentages for $\delta > 50°$.

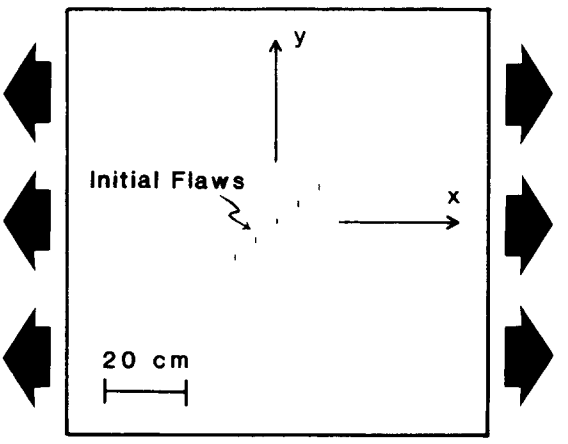

Fig. 13. The initial flaw geometry for the numerical experiments illustrating how sigmoidal fracture shapes can evolve independent of a shear zone. Initial stress boundary conditions are defined in the text. The incremental uniaxial strain in x due to the imposed boundary displacements, $\varepsilon_{xx} = 3.1 \times 10^{-4}$, starts fracture propagation.

Sigmoidal veins

Pollard *et al.* (1982) and Nicholson & Pollard (1985) have suggested that the sigmoidal shapes of veins in en échelon arrays can result from their curved propagation paths as influenced by mechanical interaction, so these shapes do not require the finite strain and rotation of a shear zone (Fig. 1b). This fact is clearly demonstrated using the elastic fracture propagation model. We examine fracture propagation in a representative volume cut out of a homogeneous, linear elastic body with a cross-sectional area of 1 m^2. The initial fracture geometry (Fig. 13) is an en échelon array with flaw length L = 1 cm, spaced at S = 5 cm, and with a fracture-array angle, $\delta = 50°$, a value just within the favored array geometry cut-off of Fig. 12. The initial remote stresses are compressive, isotropic and of constant magnitude ($\sigma^r_{xx} = -p$, $\sigma^r_{yy} = -p$, $\sigma^r_{xy} = 0$, $\sigma^c_{yy} = -p$, $\sigma^c_{xy} = 0$). The internal fluid pressure, p, is equal to the remote stress magnitude and stays constant throughout fracture propagation. The physical properties are representative of a limestone, with Young's modulus E = 60 GPa, a Poisson's ratio $\nu = 0.25$ (Clark 1966), and a fracture toughness of 2.7 MPa-m$^{1/2}$ (Atkinson & Meredith 1987).

Fracture propagation is started by imposing a fixed normal displacement of 0.0155 cm on the boundaries of the body in x and zero displacement y (Fig. 13). The values of the applied remote strains resultant from the imposed displacements at the edges of the body are $\varepsilon^r_{xx} = \varepsilon^r_1 = 3.1 \times 10^{-4}$, $\varepsilon^r_{yy} = \varepsilon^r_2 = 0$, and $\gamma^r_{max} = (\varepsilon^r_1 - \varepsilon^r_2) = 3.1 \times 10^{-4}$. This results in a crack tip stress intensity of 2.76 MPa-m$^{1/2}$ which satisfies the propagation criterion. The shear stress on the bounding surfaces was maintained at zero so the body could freely expand in the x direction in response to the applied normal displacements. Figure 14 illustrates the sequence of fracture propagation at three different stages. Initial fracture growth is essentially perpendicular to the applied extension (Fig. 14a), but as the fractures overlap and interact, their propagation paths deviate from planar to sigmoidal shapes (Figs. 14 b & c). Subsequent growth is not aligned

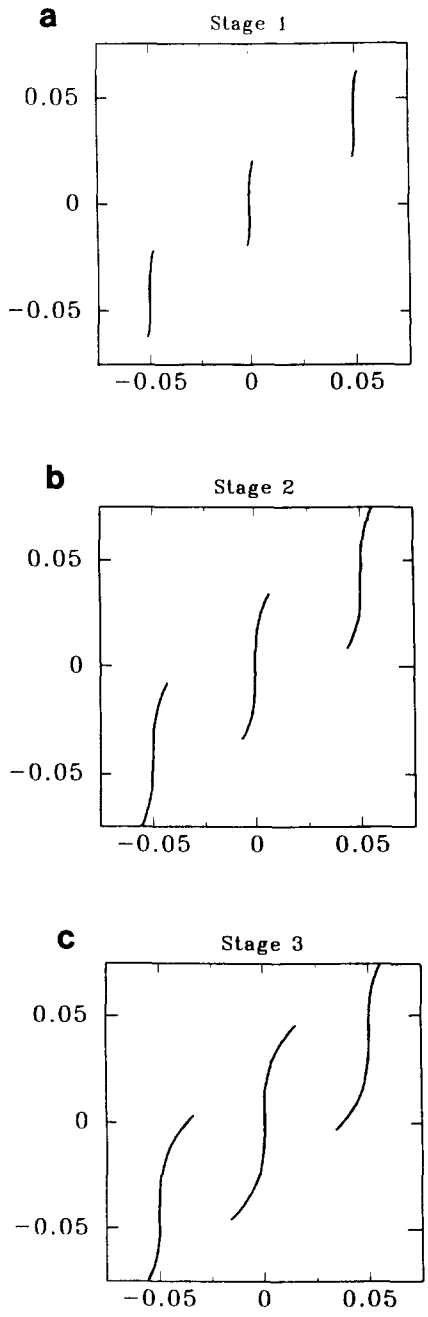

Fig. 14. Three stages in the growth of sigmoidal fractures under an incremental uniaxial extension in x (see Fig. 13). (a) Propagation approximately perpendicular to extension along nearly planar paths. (b) Curved paths begin as fractures mechanically interact. (c) Final sigmoidal shapes.

perpendicular to the remote applied extension, but is controlled by the orientation of the local stress (and strain) field.

Figure 15 depicts components of the local strain field near the center of the fracture array at stage 2 in the growth sequence. The strain field is non-homogeneous in space and time due to the presence of the propagating fractures, although the remote strains near the boundaries of the body are constant. Each increment of propagation is perpendicular to the maximum circumferential stress near the fracture tip, which corresponds to the maximum circumferential extension for our case of infinitesimal strain. For example, continued propagation of the fractures along curving paths toward their neighbors can be deduced by looking at the tick marks in Fig. 15(a), which show the direction of the maximum principal extension, ε_1.

Given that we know the fracture array of Figs. 13–15 grew in response to the deformation of an elastic solid, we can make several generalizations useful for the field interpretation of these types of structures. The remote principal strain and stress orientations are recorded only by the central portions of the fractures which propagated prior to significant mechanical interaction with other nearby fractures. For this numerical experiment, the remote principal extension direction was along the x-axis, and correspondingly the veins in Fig. 14 initially grew perpendicular to that direction. The sigmoidal

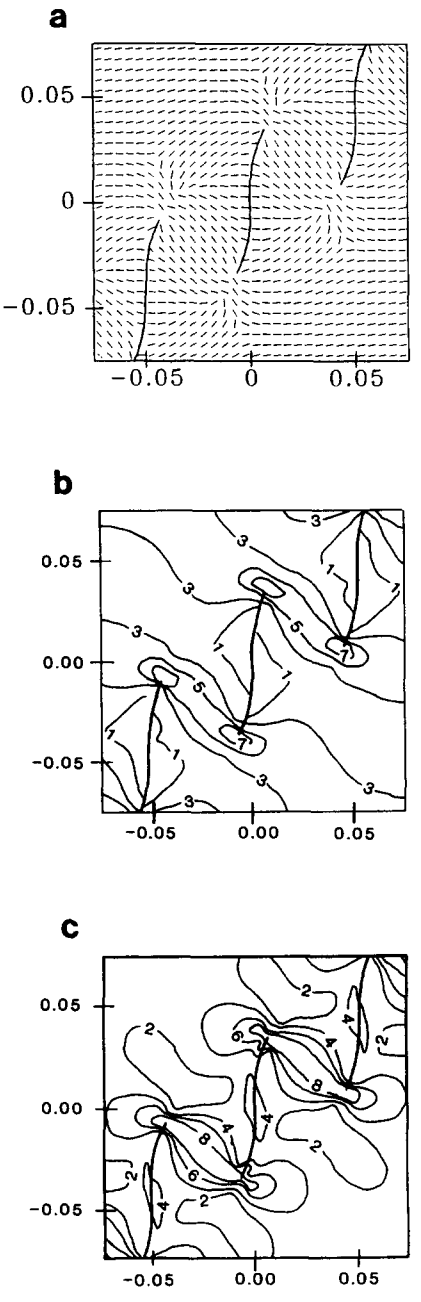

Fig. 15. Certain components of the strain field near en échelon fractures at stage 2 of the growth sequence shown in Fig. 14. These figures illustrate the heterogeneous nature of these fields. (a) Trajectories of maximum principal strain, ε_1. (b) Magnitudes of ε_1 (multiplied by 10^4). (c) Magnitudes of the maximum shear strain, γ_{max} (multiplied by 10^4).

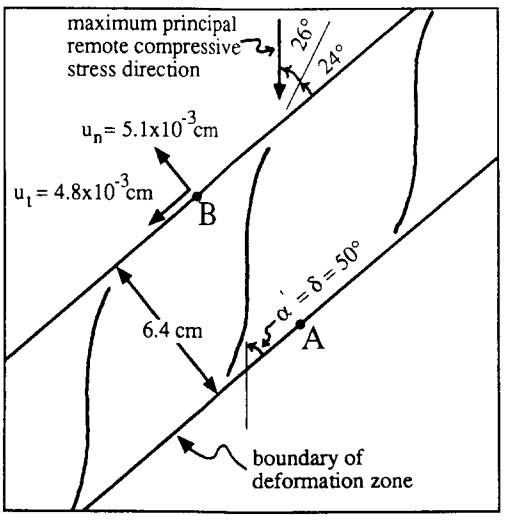

Fig. 16. En échelon fracture zone taken from stage 2 of the brittle elastic process illustrated in Fig. 14 and used here to compare the displacement and strains with those from a ductile shear zone containing a similar array of fractures. Displacement components of point B relative to point A are u_n and u_t.

shapes of the fractures after overlap do not reflect changes in the remote strain field but indicate that the differential compressive stress acting parallel to the initial fractures was not very large compared to the driving stress available for propagation, $\Delta\sigma_I$ (Olson & Pollard 1989). In addition, if minimum fracture opening displacements are recorded by mineral fillings, we can estimate the ratio of the driving stress to the elastic moduli of the material, E and ν, using the equation for opening displacement at the center of an isolated fracture,

$$\frac{1-\nu^2}{E}\Delta\sigma_I = \frac{\Delta u_I}{4a}, \tag{8}$$

where Δu_I is the opening displacement at the vein center and a is the vein half-length. If the elastic moduli can be estimated for the time of fracturing, we can actually calculate the magnitude of the driving stress, as has been done for joints (Segall & Pollard 1983) and dikes (Delaney & Pollard 1981, Pollard 1987). If the material properties during fracture propagation were not elastic, a similar analysis could still be done with continuum and fracture mechanics, but the constitutive laws would be different. For example, there are solutions in the engineering mechanics literature for fracture growth in viscoelastic materials (Graham 1969, Knauss 1974, Schapery 1975a,b) that might be applicable for cases involving larger strains and wider vein openings than those considered here.

Comparison of sigmoidal fracture analysis methods

Since the fracture array depicted in Fig. 16 (redrawn from Fig. 14b) is geometrically similar to some vein arrays attributed to shear zone deformation, and remembering that independent evidence confirming vein formation mechanism is often lacking (Shainin 1950, Rothery 1988), it is conceivable that vein arrays formed by brittle elastic fracture propagation might be misinterpreted using techniques for ductile shear zones and vice versa. An analysis follows to show the magnitude of the quantitative errors involved if the controlling deformation mechanism is not recognized.

We define the deformation zone as the extent of the en échelon array, giving a zone width of about 6.4 cm (Fig. 16). Relative to point A on the lower boundary of the zone, the displacement components of point B are $u_n = 5.12 \times 10^{-3}$ cm (normal) and $u_t = 4.79 \times 10^{-3}$ cm (tangential). The shear strain parallel to the zone is calculated from the tangential displacement and zone width as

$$\gamma = \frac{4.79 \times 10^{-3}\,\text{cm}}{6.4\,\text{cm}} = 7.48 \times 10^{-4}. \tag{9}$$

The resultant shear strain parallel to the zone in the remote field is 1.53×10^{-4}, showing that the deformation is increased in the vicinity of the fracture array.

If we look only at the central portions of the fractures and mistakenly interpret that they rotated passively as lines during ductile shear deformation, we will calculate an incorrect shear strain accommodated in the zone since fracture initiation. Shear strain, $\gamma = \cot\alpha - \cot\alpha'$, is related to the rotation of a line segment in homogeneous simple shear (Ramsay & Huber 1983, p. 24), where α is the original angle between the line and the shear zone boundary and α' is the final angle of the rotated line. Shear strain is positive for anticlockwise rotation and negative for clockwise. According to the simple shear model, fractures formed during the initial increment of shear displacement would be oriented perpendicular to the maximum extension, that is at $\alpha = 45°$ for this left-lateral zone. From Fig. 16 the passive rotation is 5° in the anticlockwise direction ($\alpha' = 50°$), resulting in a shear strain of

$$\gamma = \cot 45° - \cot 50° = 0.161.$$

This is over two orders of magnitude greater than the shear strain calculated for the brittle elastic zone.

Lajtai (1969) suggests that the orientation of the remote maximum principal compressive stress can be inferred to be parallel to the tips of sigmoidal veins where these veins have propagated outside the boundary of a shear zone. Durney & Ramsay (1973, Fig. 15) reiterate this idea and describe how progressive deformation in a shear zone causes passive rotation of the vein body while propagation at the tip continues perpendicular to the incremental stretch direction, that is at 45° from the zone boundary. However, the orientation of the fracture tips in Fig. 16 are at 24° to the zone boundary, and 26° from the remote maximum principal stress orientation used to generate the fracture array.

Ramsay & Huber (1983, pp. 48–50) suggest that a combination of homogeneous simple shear and dilatation (actually they impose a longitudinal strain perpendicular to the shear zone boundary) can be used to explain veins that are initially oriented at an angle different from 45° or 135° in left- or right-lateral shear

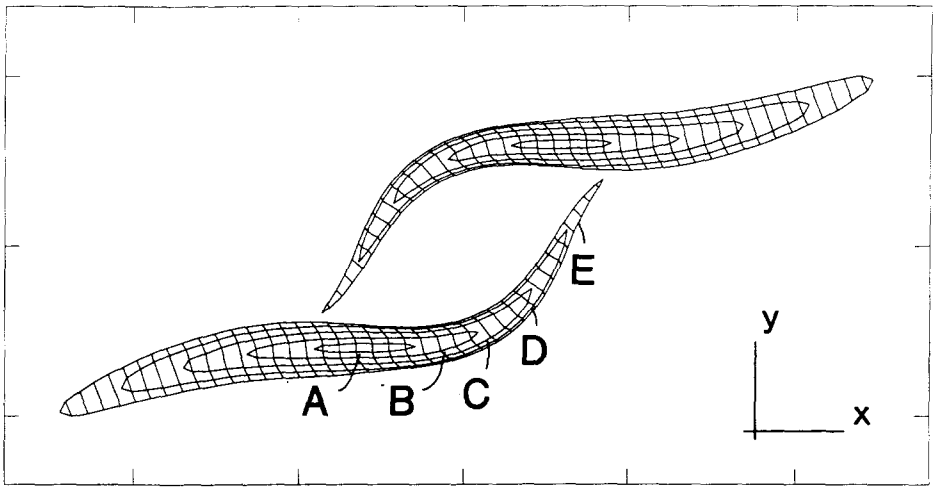

Fig. 17. Fracture path and elastic wall displacements for a fluid-pressurized fracture experiencing a fracture-parallel differential compressive stress equal to one-tenth the driving stress. Closed contours A–E denote positions of the fracture walls at five stages of growth. Transverse lines cross-cutting fractures show the opening and shearing displacement paths of initially adjacent points on opposing fracture walls.

zones, respectively. Addition of a positive dilation (extension across the zone) rotates the strain ellipse such that the maximum extension is at a greater angle to the zone boundary. A negative dilation (contraction across the zone) results in a lesser angle. By equating the strain ellipse's long axis with the normal to extension fractures they interpret en échelon arrays with $\delta < 45°$ as indicating positive dilation and those with $\delta > 45°$ as indicating negative dilation for left lateral shear zones. They give numerical examples for $\delta = 24°$ and $\delta = 69°$ that arise from a shear strain, $\gamma = 0.1$, and dilations of $\Delta_A = +0.1$ and $\Delta_A = -0.1$, respectively. This relationship between dilation and vein angle does not hold for the example of Fig. 16. Assuming no stretching in the direction parallel to the zone, the area change (dilation) is

$$\Delta_A = \frac{5.12 \times 10^{-4}\,\text{cm}}{6.4\,\text{cm}} = 8 \times 10^{-4}.$$

Not only is the strain orders of magnitude smaller than those for the ductile shear zone example, the sign of the dilation is the opposite of what is predicted by Ramsay & Huber (1983) for veins with $\delta > 45°$. In addition, the fracture geometries of Fig. 9 illustrate how δ can range from near 0° to over 50° (Fig. 12) in a body subject to a single remote stress and strain field. The variation in vein-array angle for the case of brittle elastic fracture propagation depends on the spatial distribution of the initial flaws and their mechanical interaction during growth.

It should be clear from this comparison that significant quantitative errors can result from the use of either model if it has been incorrectly applied to a natural fracture array.

Fibrous vein fillings

Durney & Ramsay (1973) and Ramsay & Huber (1983, fig. 13.1) suggested that the displacement of fracture walls as indicated by fibrous vein fillings can be used to infer the progression of incremental strain axis directions during fracture growth. Sigmoidally shaped syntaxial and antitaxial vein fibres track fracture wall opening and shearing displacements. Our next example investigates the use of sigmoidal vein fillings to infer fracture wall displacements and then to interpret the direction of the incremental strain axes.

To illustrate the role of mechanical interaction on fracture wall displacements, we consider two parallel en échelon fractures that propagate toward one another and overlap, following a convergent propagation path as determined by the fracture tip stress field (Pollard *et al.* 1982, Olson & Pollard 1989). The remote strain (and stress) state was constant in orientation with principal axes parallel to x and y. The remote strain (and stress) magnitudes were also constant throughout propagation, with a constant compressive differential stress along the x axis equal to one-tenth the 1 MPa driving pressure. Therefore, any shear offset of fracture walls or propagation path curving is not the result of changes in the orientation of the remote principal strain axes, but a response to the heterogeneity of the local strain due to mechanical interaction of the two fractures.

Figure 17 shows the location of the fracture walls at five different stages (A–E) during the numerical experiment. The elastic opening has been exaggerated for illustration purposes by using a small Young's modulus, $E = 25$ MPa, three orders of magnitude less than what is typically expected for most rock. The transverse lines are displacement vectors that track the movement of previously adjacent points on the fracture walls. Initially (stage A), both fractures follow straight paths and the wall displacements are nearly pure opening because the fractures are symmetric with respect to the remote strain field and too far apart relative to their lengths to interact significantly. In the second stage of growth (B), the inner tips curve toward one another signalling the beginning of fracture interaction. The walls now exhibit a small shear offset at the center of each fracture, but the displace-

ment near the tips is still pure opening. Further left-lateral offset at the fracture center occurs during growth stages C and D, as the inner tips follow a smoothly curving convergent path. Growth stage E signals a change in the propagation path as the inner tips begin to curve in the opposite sense. This has a curious effect on the wall displacements—the incremental shear offset changes to right-lateral for most of the overlapping portion of the fractures, indicating a change in the sense of the local fracture-induced shear resolved on the overlapping fracture segments.

The results of Fig. 17, we suggest, are an analog for antitaxial fibre growth accompanying the propagation and dilation of veins. The displacement vectors record a complex history that reflects significant changes in the local strain (and stress) state due to mechanical interaction. If mineral fibres were to grow parallel to these vectors their long dimensions would have to rotate as much as 20° from the middle to the wall of the vein. The fibers near the vein tips would be straighter than those at the center, a geometry that has been observed in natural veins (Ramsay & Huber 1983, figs. 13.14 and 13.15). It is important to note that although this example has curving vein traces, Pollard *et al.* (1982) showed that similar shear offsets of the fracture wall can occur in overlapping fractures that follow straight paths. Using a more realistic rock modulus (of the order of 10^5 MPa) to calculate the deformations in Fig. 17 would have no effect on the fracture propagation paths. The fracture wall displacements would have the same proportion of opening to shearing, but the magnitudes would be greatly diminished. These displacements are inversely proportional to elastic modulus.

It should be clear from this example that there is no necessary correspondence between vein fiber orientation or fracture tip orientation and that of the remote incremental strain axes. In this case only the early stages of vein propagation and opening are aligned with the remote principal strains. We have also shown that the rotation of the remote principal strain or stress components is not a necessary condition for sigmoidal vein features. The remote field and that induced by the fracture interaction combine to determine the propagation direction and wall displacement history.

DISCUSSION

We propose the following model for en échelon vein array development. The rock mass has local points of stress concentration caused by flaws and heterogeneities that are randomly located and oriented (Fig. 18a). Pollard & Aydin (1988) describe a variety of such stress concentrators typically found in rock and explain why fractures that initiate at these points will grow preferentially perpendicular to the least compressive remote (regional) stress. Due to the action of these pre-existing flaws, a population of randomly distributed but subparallel micro-cracks develop in the rock body (Fig. 18b). Fluids in the rock mass may fill these fractures and deposit minerals to form veins. As the veins become long enough to mechanically interact with one another, growth becomes more selective, causing the members of stacked arrays to slow or stop while members of en échelon arrays experience enhanced growth (Fig. 18c). Veins with $\delta < 50°$ would start growing at approximately the conditions depicted by the curve for $S/L_o = 10$ (Fig. 12) and move to greater propagation ratios as S/L_o decreases. In contrast, for $\delta > 50°$, decreasing S/L_o ratios correspond to decreasing propagation ratios. Thus, the rock mass is cut by veins of various lengths and positions, but many of them occur in en échelon arrays.

En échelon arrays may be zones of weakness in the rock body (Fig. 18d), depending on the nature of the vein filling minerals, and, as such, they would localize subsequent deformation. The array could enhance strain by lowering of the rock's shear modulus (Lajtai 1969, Casey 1980). The deformation could consist of the buckling of inter-vein columns of rock analogous to deformation observed in laboratory specimens (Peng & Johnson 1972) or in kink bands (Segall & Pollard 1983). Through fracturing between en échelon veins, deformation could cause the formation of small faults whose length would increase as more en échelon fractures link up (Roering 1968, Segall & Pollard 1983, Martel *et al.* 1988). Ductile shear zones might also form, utilizing the weakened zone of an en échelon array and passively rotating pre-existing veins into a sigmoidal pattern (Roering 1968).

We have reviewed the two existing mechanisms for en échelon vein formation and introduced a third. In principle, the different deformation mechanisms can be

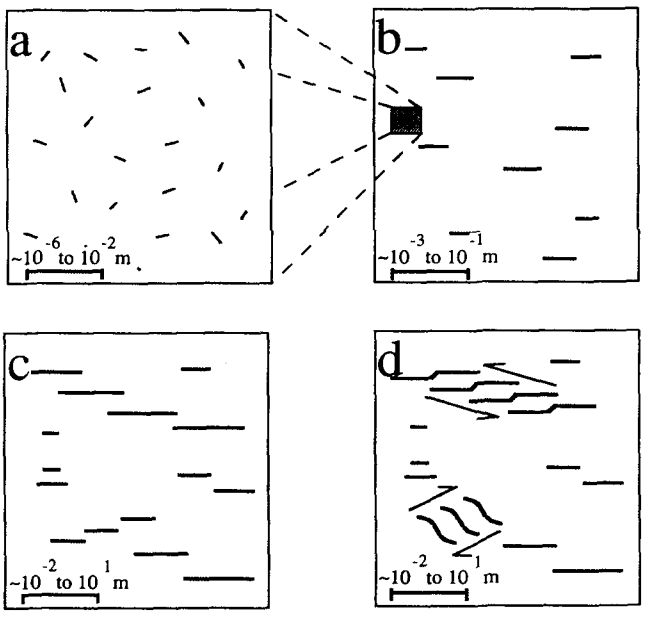

Fig. 18. Vein growth sequence. (a) Randomly located and oriented grain-scale flaws in a rock mass. (b) Flaws grow into micro-cracks that align perpendicular to the least compressive principal stress. (c) Fractures become long enough relative to their separation to interact, and selective vein growth due to this interaction favors the development of en échelon arrays. (d) Subsequent (more severe) deformation may modify the vein configuration of C by localizing shearing along pre-existing zones of weakness defined by en échelon arrays.

distinguished by careful observations when guided by model studies of the kind described here. Accurate interpretation of en échelon veins relies upon the identification of diagnostic structural features that can be linked with one of these mechanisms. For example, a finite shear strain will leave evidence of shear offset if any markers cross the boundaries of the zone, but such markers are often absent. Breakdown of a parent fracture into en échelon segments can be confirmed by locating the parent fracture, yet this is often difficult because of the two-dimensional nature of many outcrops. A wide range of vein-array angles for en échelon veins with contemporaneous sub-parallel isolated veins in the same region supports the mechanism of selective opening fracture growth from random flaws, but timing relationships are often difficult to establish.

The possibility of multiple episodes of veining in response to differently oriented principal strains may complicate interpretations considerably, so it is important to determine the relative ages of all fracture sets and examine those of different ages separately. Determining the timing of finite deformation relative to the onset of vein growth also is important, as the possibility exists that en échelon veins form early and provide zones of weakness along which later deformation is localized.

Acknowledgements—This material is based upon work supported by the National Science Foundation under grant EAR-8707314.

REFERENCES

Atkinson, B. K. & Meredith, P. G. 1987. Experimental fracture mechanics data for rocks and minerals. In: *Fracture Mechanics of Rock* (edited by Atkinson, B. K.). Academic Press, London, 477–526.

Bankwitz, P. 1965. Über klufte I. Beobachtungen im Thuringischen Schiefergebirge. *Geologie* **14**, 241–253.

Beach, A. 1975. The geometry of en echelon vein arrays. *Tectonophysics* **28**, 245–263.

Brace, W. F. & Bombolakis, E. G. 1963. A note on brittle crack growth in compression. *J. geophys. Res.* **68**, 3709–3713.

Brace, W. F., Paulding, B. W. & Scholz, C. 1966. Dilatancy in the fracture of crystalline rocks. *J. geophys. Res.* **71**, 3939–3953.

Casey, M. 1980. Mechanics of shear zones in isotropic dilatant materials. *J. Struct. Geol.* **2**, 143–147.

Clark, P., Jr. 1966. Handbook of physical constants. *Mem. geol. Soc. Am.* **97**, 587.

Cloos, E. 1955. Experimental analysis of fracture patterns. *Bull. geol. Soc. Am.* **66**, 241–258.

Craddock, J. P. & van der Pluijm, B. A. 1988. Kinematic analysis of an en échelon–continuous vein complex. *J. Struct. Geol.* **10**, 445–452.

Crouch, S. L. & Starfield, A. M. 1983. *Boundary Element Methods in Solid Mechanics*. George Allen and Unwin, London.

Delaney, P. T. & Pollard, D. D. 1981. Deformation of host rocks and flow of magma during growth of Minette dikes and breccia-bearing intrusions near Ship Rock, New Mexico. *Prof. Pap. U.S. geol. Surv.* **1202**.

Dey, T. N. & Wang, C. 1981. Some mechanisms of microcrack growth and interaction in compressive rock failure. *Int. J. Rock Mech. & Mining Sci.* **18**, 199–209.

Dunn, D. E., Lafountain, L. J. & Jackson, R. E. 1973. Porosity dependence and mechanism of brittle fracture in sandstones. *J. geophys. Res.* **78**, 2403–2417.

Durney, D. W. & Ramsay, J. G. 1973. Incremental strains measured by syntectonic crystal growth. In: *Gravity and Tectonics* (edited by DeJong, K. A. & Scholten, R.). Wiley, New York, 67–96.

Erdogan, F. & Sih, G. C. 1963. On the crack extension in plates under plane loading and transverse shear. *Trans. Am. Soc. Mech. Engrs* **85**, 519–527.

Graham, G. A. C. 1969. The solution of mixed boundary value problems that involve time-dependent boundary regions for viscoelastic materials with one relaxation function. *Acta Mech.* **8**, 188–204.

Granier, T. 1985. Origin, damping, and pattern development of faults in granite. *Tectonics* **4**, 721–737.

Hallbauer, D. K., Wagner, H. & Cook, N. G. W. 1973. Some observations concerning the microscopic and mechanical behavior of quartzite specimens in stiff, triaxial compression tests. *Int. J. Rock Mech. & Mining Sci.* **10**, 713–726.

Hancock, P. L. 1972. The analysis of en echelon veins. *Geol. Mag.* **109**, 269–276.

Hodgson, R. A. 1961. Classification of structures on joint surfaces. *Am. J. Sci.* **259**, 493–502.

Ingraffea, A. R. 1981. Mixed-mode fracture initiation in Indiana limestone and Westerly Granite. *Proc. 22nd Symp. Rock Mechanics*, 186–191.

Knauss, W. G. 1974. On the steady propagation of a crack in a viscoelastic sheet: Experiments and analysis. In: *Deformation and Fracture of High Polymers* (edited by Knauss, H. H. *et al.*). Plenum, New York, 501–541.

Knipe, R. J. & White, S. H. 1979. Deformation in low grade shear zones in the Old Red Sandstone, S.W. Wales. *J. Struct. Geol.* **12**, 53–66.

Kranz, R. L. 1979. Crack–crack and crack–pore interactions in stressed granite. *Int. J. Rock Mech. & Mining Sci.* **16**, 37–47.

Kranz, R. L. 1983. Microcracks in rocks: A review. *Tectonophysics* **100**, 449–480.

Lajtai, E. Z. 1969. Mechanics of second order faults and tension gashes. *Bull. geol. Soc. Am.* **80**, 2253–2272.

Lawn, B. R. & Wilshaw, T. R. 1975. *Fracture of Brittle Solids*. Cambridge University Press, Cambridge.

Martel, S. J., Pollard, D. D. & Segall, P. 1988. Development of simple strike-slip fault zones, Mount Abbott Quadrangle, Sierra Nevada, California. *Bull. geol. Soc. Am.* **100**, 1451–1465.

Nicholson, R. & Pollard, D. D. 1985. Dilation and linkage of echelon cracks. *J. Struct. Geol.* **7**, 583–590.

Olson, J. & Pollard, D. D. 1989. Inferring paleostresses from natural fracture patterns: A new method. *Geology* **17**, 345–348.

Olsson, W. A. & Peng, S. S. 1976. Microcrack nucleation in Marble. *Int. J. Rock Mech. & Mining Sci.* **13**, 53–59.

Peng, S. & Johnson, A. M. 1972. Crack growth and faulting in cylindrical specimens of Chelmsford Granite. *Int. J. Rock Mech. & Mining Sci.* **9**, 37–86.

Pollard, D. D. 1987. Elementary fracture mechanics applied to the structural interpretation of dykes. In: *Mafic Dyke Swarms* (edited by Hall, H. C. & Fahrig, W. F.). *Spec. Pap. geol. Ass. Can.* **34**, 5–24.

Pollard, D. D. & Aydin, A. 1988. Progress in understanding jointing over the past century. *Bull. geol. Soc. Am.* **100**, 1181–1204.

Pollard, D. D. & Segall, P. 1987. Theoretical displacement and stresses near fractures in rock: with applications to faults, joints, veins, dikes, and solution surfaces. In: *Fracture Mechanics of Rock* (edited by Atkinson, B. K.). Academic Press, London, 277–350.

Pollard, D. D., Segall, P. & Delaney, P. 1982. Formation and interpretation of dilatant echelon cracks. *Bull. geol. Soc. Am.* **93**, 1291–1303.

Ramsay, J. G. 1980. The crack-seal mechanism of rock deformation. *Nature* **284**, 135–139.

Ramsay, J. G. & Huber, M. I. 1983. *The Techniques of Modern Structural Geology, Volume* 1: *Strain Analysis*. Academic Press, London.

Rickard, M. J. & Rixon, L. K. 1983. Stress configurations in conjugate quartz-vein arrays. *J. Struct. Geol.* **5**, 573–578.

Riedel, W. 1929. Zur mechanik geologischer Brucherscheinungen (Ein Beitrag zum Problem der Fiederspatten). *Zentbl. Miner. Geol. Paläeont. Abh.* **B**, 354–368.

Roering, C. 1968. The geometrical significance of natural en echelon crack arrays. *Tectonophysics* **5**, 107–123.

Rothery, E. 1988. En échelon vein array development in extension and shear. *J. Struct. Geol.* **10**, 63–71.

Sangha, C. M., Talbot, C. J. & Dhir, R. K. 1974. Microfracturing of a sandstone in uniaxial compression. *Int. J. Rock Mech. & Mining Sci.* **11**, 107–113.

Schapery, R. A. 1975a. A theory of crack initiation and growth in viscoelastic media I. Theoretical development. *Int. J. Fract.* **11**, 141–159.

Schapery, R. A. 1975b. A theory of crack initiation and growth in viscoelastic media II. Analysis of continuous growth. *Int. J. Fract.* **11**, 549–562.

Segall, P. 1984. Formation and growth of extensional fracture sets. *Bull. geol. Soc. Am.* **95**, 454–462.

Segall, P. & Pollard, D. D. 1983. Joint formation in granitic rock of the Sierra Nevada. *Bull. geol. Soc. Am.* **94**, 563–575.

Shainin, V. E. 1950. Conjugate sets of en echelon tension fracture in the Athens limestone at Riverton, VA. *Bull. geol. Soc. Am.* **61**, 509–517.

Shaoxun, H. & Xiaoshuang, X. 1988. The origin of echelon structures of Tungsten veins in Xishuashan, Jiangxi. *Acta Geol. Sinica* **1**, 267–280.

Sobolev, G., Spetzler, H. & Salov, B. 1978. Precursors to failure in rocks while undergoing anelastic deformations. *J. geophys. Res.* **83**, 1775–1784.

Sommer, E. 1969. Formation of fracture lances in glass. *Engng Fract. Mech.* **1**, 539–546.

Tapponier, P. & Brace, W. F. 1976. Development of stress induced microcracks in Westerly granite. *Int. J. Rock Mech. & Mining Sci.* **13**, 102–112.

Timoshenko, S. P. & Goodier, J. N. 1970. *Theory of Elasticity*. McGraw-Hill, New York.

Wilson, G. 1952. A quartz vein system in the Moine Series near Melness, A'Mhoine, North Sutherland, and its tectonic significance. *Geol. Mag.* **89**, 141–144.

Wong, T. F. 1982. Micromechanics of faulting in Westerly Granite. *Int. J. Rock Mech. & Mining Sci.* **19**, 49.

Woodworth, J. B. 1896. On the fracture system of joints, with remarks on certain great fractures. *Proc. Boston Soc. Nat. Hist.* **27**, 163–183.